A Letters Journal Exploring the Frontiers of Physics

July 2008

EPL, **83** (2008) 15003
doi: 10.1209/0295-5075/83/15003

www.epljournal.org

Evolution of the radial electric field in a JET H-mode plasma

Y. Andrew[1,2], N. C. Hawkes[1,2], T. Biewer[1,3], K. Crombe[1,4], D. Keeling[1,2], E. de la Luna[1,5], C. Giroud[1,2], A. Korotkov[1,2], A. Meigs[1,2], A. Murari[1,6], I. Nunes[1,7], R. Sartori[1,8], T. Tala[1,9] and JET-EFDA contributors[1(a)]

[1] *JET-EFDA, Culham Science Centre - Abingdon, OX14 3DB, UK, EU*
[2] *Euratom/UKAEA Fusion Association, Culham Science Centre - Abingdon, OX14 3DB, UK, EU*
[3] *Oak Ridge National Laboratory - Oak Ridge, TN 37831, USA*
[4] *Department of Applied Physics, Ghent University - Belgium, EU*
[5] *Asociasion EURATOM-CIEMAT para Fusion, CIEMAT - Madrid, Spain, EU*
[6] *Consorzio RFX, ENEA-Euratom Association - Padua, Italy, EU*
[7] *Associação EURATOM/IST, Centrode Fusão Nuclear - Lisbon, Portugal, EU*
[8] *EFDA CSU - Boltzmannstrasse 2, 85748 Garching, Germany, EU*
[9] *Association EURATOM-Tekes, VTT - P.O. Box 1000, FIN-02044 VTT, Finland, EU*

received 27 March 2008; accepted in final form 20 May 2008
published online 16 June 2008

PACS 52.30.-q – Plasma dynamics and flow

Abstract – Results from recent measurements of carbon impurity ion toroidal and poloidal rotation velocities, ion temperature, ion density and the resulting radial electric field (E_r) profiles are presented from an evolving Joint European Torus (JET) tokamak plasma over a range of energy and particle confinement regimes. Significant levels of edge plasma poloidal rotation velocity have been measured for the first time on JET, with maximum values of $\pm 9\,\mathrm{km\,s^{-1}}$. Such values of poloidal rotation provide an important contribution to the total edge plasma E_r profiles. Large values of shear in the measured E_r profiles are observed to arise as a consequence of the presence of the edge transport barrier (ETB) and do not appear to be necessary for their formation or destruction. These results have an important impact on potential mechanisms for transport barrier triggering and sustainment in present-day and future high-performance fusion plasmas.

Introduction. – The current operation scenario envisaged for the next step magnetic fusion device, ITER [1], is one with high energy and confinement times, the H-mode. Despite large progress in the development of the H-mode regime on tokamaks worldwide, an understanding of the triggering and sustainment mechanisms for the Low-to-High confinement regime (L-H) transition, various H-mode phases and the High-to-Low confinement phase (H-L) transitions remains elusive. A great deal of the theoretical and experimental research has concentrated on the role of the radial electric field, E_r, at the L-H transition, for example see [1–5] and references therein. Large gradients in the edge E_r are considered to lead to shear in the plasma $\mathbf{E}\times\mathbf{B}$ flow which effectively breaks up turbulent eddies and reduces cross-field transport. The edge transport barrier subsequently forms, leading to the improved plasma energy, particle and momentum confinement times characteristic of the H-mode. Experimental studies have shown that gradients in E_r persist throughout H-modes and are a general experimental feature of plasmas with an edge transport barrier. Results are presented in this paper from recent work to focus on this particular process, by considering the evolution of the measured impurity ion toroidal (v_ϕ) and poloidal (v_θ) rotation velocities and their contribution to the edge E_r, via the force balance equeation described below, over the changing phases of an H-mode plasma on the Joint European Torus (JET) tokamak.

Earlier experimental work in this area include very highly resolved measurements of E_r at the plasma edge for a wide range of H-mode discharges on DIII-D [2]. A well-like structure was observed in E_r at the L-H transition in all plasmas. All the measured E_r wells were negative with nearly the same spatial width, but differences in depth and under all conditions the shear in the E_r profile persisted throughout the H-mode. The greatest contribution to E_r came from changes in impurity poloidal rotation

[(a)] See the appendix of Watkins M. L. *et al.*, *Fusion Energy 2006, Proceedings of the 21st International Conference, Chengdu, 2006* (IAEA) 2006.

velocity, v_θ, while the influence of the diamagnetic term only became appreciable tens of milliseconds into the H-mode as the ion pressure increased. The sign of carbon ion v_θ was also observed to be consistently in the electron diamagnetic direction. More recent DIII-D measurements of v_θ profiles have been reported in [4] for Quiescent H-modes. Charge Exchange Recombination Spectroscopy (CXRS) on carbon and neon impurity species, was used to measure the E_r profile across the core and edge plasma. Following the application of velocity corrections due to the energy-dependent cross-sections and ion gyromotion, the experimental poloidal rotation profiles for both impurity species were found to be significantly greater than predictions of v_θ. Previous JET studies by Hawkes *et al.* [6] have shown no evidence of changes in the impurity v_θ at the L-H transition, or during established H-modes. Although this previous work demonstrates that the edge E_r is strongly affected by the L-H transition, it is not clear whether the gradient in the E_r profile is the cause or consequence of improved confinement in the H-mode.

Recent enhancements to the JET edge plasma CXRS diagnostic have returned it to a balanced up-down symmetrical view of the neutral beam injection [7–9]. These changes together with new detectors allow accurate measurements of the impurity ion v_θ, v_ϕ, ion temperature, T_i, and ion density, n, profiles, with fine spatial resolution across the pedestal region. This letter presents the first detailed measurements of the evolution of the edge plasma E_r profile and its contributing terms over all phases of a non-stationary JET H-mode plasma. The example plasma presented in this letter has been chosen since it covers many different phases of L- and H-mode regimes and is a good representation of what is generally observed on JET with the improved diagnostic.

Experiment. – The evolution of the edge plasma rotation and E_r is examined for pulse # 69937, a single null configuration with the ion ∇B drift towards the magnetic null-point, $I_p/B_t = 2.5\,\mathrm{MA}/2.7\,\mathrm{T}$ and $q_{95} = 3.3$. This plasma had relatively high shaping and a divertor configuration such that the inner strikepoint remained on the inner vertical target, while the outer strikepoint location was on the outer horizontal target. The various H-mode transitions were accessed by slowly ramping the neutral beam power up and then back down at a rate of $1\,\mathrm{MW\ s^{-1}}$, as shown in fig. 1. A constant level of 1 MW of Ion Cyclotron Resonance Heating (ICRH) power was applied throughout the beam heating phase. The L-mode plasma n_e was controlled using active gas feedback on the deuterium fuelling, also shown in fig. 1, which led to variation of the level of gas puffing throughout the shot.

According to the force balance equation, E_r can be written as

$$E_r = \nabla P/neZ + v_\phi B_\theta - v_\theta B_\phi, \qquad (1)$$

where P is the ion pressure, Z is the ion charge number, e is the electron charge, n is the ion density, v_ϕ and v_θ are the toroidal and poloidal velocities, respectively and B_ϕ and B_θ are the toroidal and poloidal magnetic fields, respectively. Equation (1) is valid for fuel and impurity ion species individually and in this paper all measurements were made with C^{6+} ions. It should be noted that the values and directions of v_ϕ and v_θ for different plasma ions can vary significantly from one another [2–5]. However, E_r and the $\mathbf{E}\times\mathbf{B}$ velocity shear, apply to all plasma species.

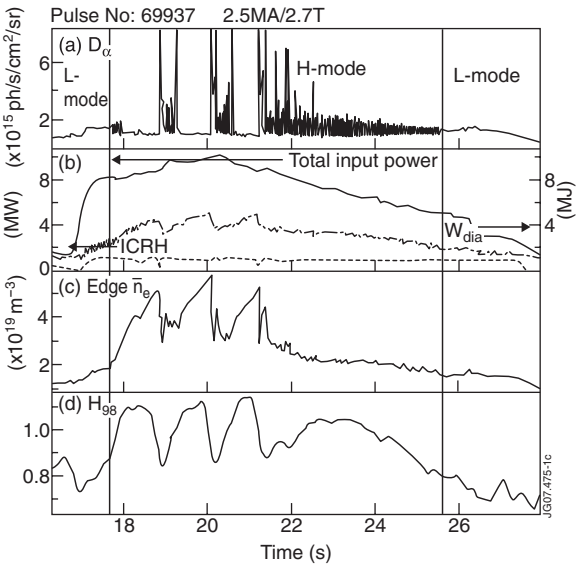

Fig. 1: General plasma parameters for shot # 69937. (a) Divertor D_α signal, (b) total input power, ICRH power and plasma energy, (c) edge electron density, $\bar{n}_e$ and (d) H-mode confinement enhancement factor, H_{98}.

The edge plasma viewing CXRS system on JET has views along fourteen radial channels locations ranging from mid-plane radius of, $R_{mid} = 3.65$–$3.85\,\mathrm{m}$ ($\rho \cong 0.65$–1.2) with spatial resolution ranging from 1.2 to 2.3 cm and temporal resolution of 50 ms. The balanced viewing geometry allows the measurements of v_ϕ and v_θ to be made self-consistently from line-of-sight velocities that have both toroidal and poloidal components. Further details on the diagnostic and its measurements can be found in [7].

The electron temperature, T_e, has been measured with a multichannel Electron Cyclotron Emission (ECE) radiometer with a time resolution of 1 ms. The electron temperature at the top of the pedestal has been identified by the discontinuity in the gradient across the pedestal as defined in [10] and as used in previous JET studies [11–13]. The T_e at the pedestal top at the L-H transition is obtained by applying the pedestal position identified at the first clear H-mode T_e pedestal, to the T_e profile at the time of the transition. The line integrated edge n_e is measured with an interferometer along a single chord at $R_{mid} = 3.74\,\mathrm{m}$ for this shot. The line average edge $\bar{n}_e$ has been calculated by dividing the measured line integrated n_e by the chord length in the plasma.

Results. – The L-H transition in this shot occurs at $t = 17.7\,\mathrm{s}$ and is characterised by the start of very small,

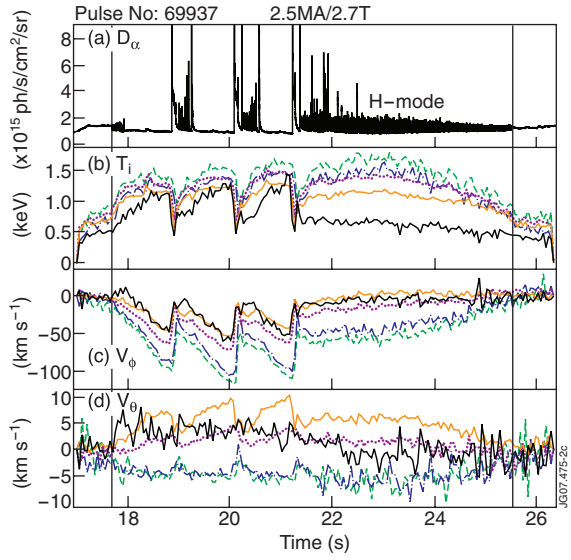

Fig. 2: Overview of the T_i, v_ϕ and v_θ across the L-mode and H-mode phases of shot # 69937 at $I_p/B_t = 2.5$ MA/2.7 T. The colour of each time trace corresponds to the radial location indicated in fig. 3 by corresponding vertical lines of the same colour.

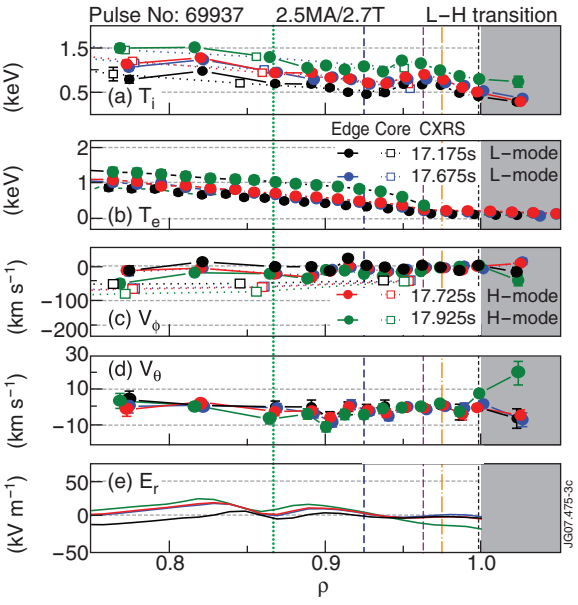

Fig. 3: Radial profiles for the edge plasma (a) T_i, (b) T_e, (c) v_ϕ and (d) v_θ and (e) E_r values across the L-H transition for shot # 69937. The vertical colour lines indicate the radial locations of the time traces in corresponding colours in figs. 2 and 4.

irregular events which degrade the edge transport barrier, known as edge localised modes (ELMs). The L-H transition is also accompanied by increased values of plasma $\bar{n}_e$, the plasma energy, W_{dia} and the plasma confinement enhancement factor, H_{98} [14], indicated by the first vertical line in figs. 1 and 2. The threshold power for access to the H-mode in this plasma was $P_{th} = 6.8$ MW at an edge density of $\bar{n}_e = 1.8 \times 10^{19}$ m^{-3}. The confinement

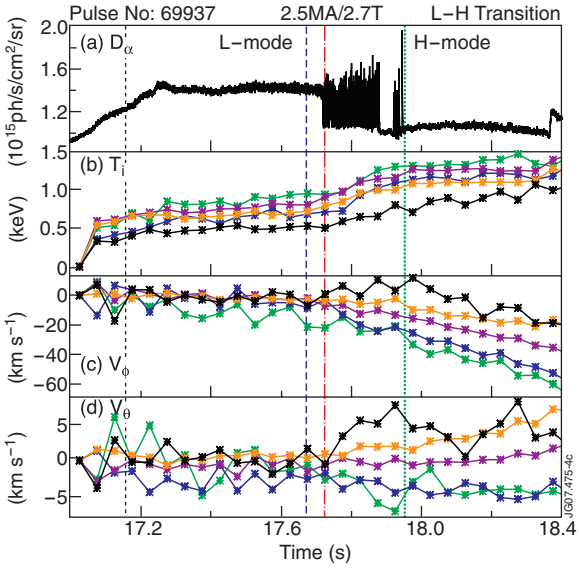

Fig. 4: Time traces showing (a) the divertor D_α signal, (b) the edge T_i, (c) edge v_ϕ and (d) edge v_θ values for radial locations indicated in fig. 3, across the L-H transition for shot # 69937.

factor directly following the L-H transition, was $H_{98} = 0.9$ and it increased to 1.0 by the end of the first short, ELMy phase. The values of T_i, v_ϕ and v_θ at radial locations indicated in fig. 3 by vertical, colour lines are plotted in their corresponding colours as a function of time in fig. 2 and in more detail in fig. 4 along with the divertor D_α signal. This method of profile and time trace cross-correlation is used throughout the letter. The radial profiles of the edge plasma T_i, T_e, v_ϕ, v_θ and E_r are plotted as a function radius normalised to the plasma radius in fig. 3 for time-slices in the L-mode phase, across the L-H transition and following the initial ELMy phase, all indicated by the corresponding vertical, colour lines in fig. 4. Measurements of T_i and v_ϕ across the core plasma are also included in the profile plots as open symbols. During the L-mode phase (black and blue profiles in fig. 3) a very small increase is observed in the T_i and T_e profiles, with the pedestal top values of $T_i = 790(\pm 22)$ eV at $\rho = 0.95$ and $T_e = 320(\pm 32)$ eV at $\rho = 0.94$ for the last L-mode time-slice. A much more significant increase in the temperature pedestals can be seen in figs. 3(a,b) and 4(b) following the transition to H-mode. The edge plasma v_θ profile remains close to zero throughout the L-mode phase as shown by the profiles in fig. 3(d) and the corresponding time traces in figs. 2(d) and 4(d). However, v_θ is observed to spin-up along the outermost two channels (green profile) after the L-H transition, to a maximum value of $8(\pm 2)$ km s^{-1} just within the last closed magnetic flux surface (LCFS). The edge v_ϕ profile also remains very flat at around 0 km s^{-1} during the L-mode phase as shown in figs. 2(c), 3(c) and 4(c). At the start of the H-mode, however, the innermost channels measure a strong increase in v_ϕ in the negative co-current direction (blue time traces), while just within the LCFS the

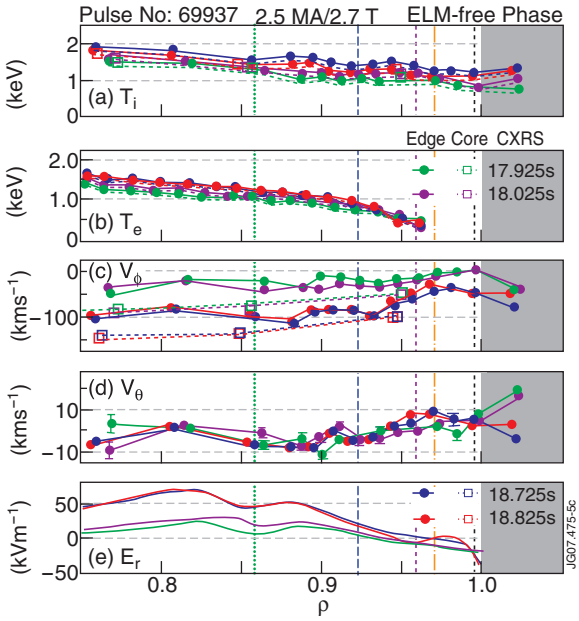

Fig. 5: Radial profiles for the time-slices indicated by vertical lines in fig. 6 in corresponding colours, in the ELM-free phase of the H-mode for shot # 69937.

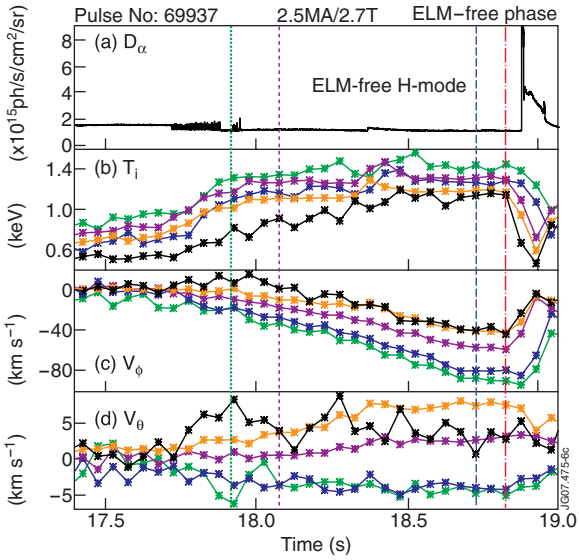

Fig. 6: Time traces across the ELM-free phase of the H-mode for shot # 69937 for (a) the divertor D_α, (b) edge T_i, (c) edge v_ϕ and (d) edge v_θ for corresponding radii indicated by vertical lines in fig. 5.

plasma briefly spins up to $12(\pm5)\,\mathrm{km\,s^{-1}}$ in the positive counter-current direction (black time-trace). Following the transition to the ELM-free phase all channels observe toroidal velocity spin-up in the co-current direction and the development of a gradient in v_θ. The corresponding E_r profiles, fig. 3(e), remain flat and close to $0\,\mathrm{kV\,m^{-1}}$ across the edge plasma in the L-mode phase. A gradient in E_r subsequently develops in the H-mode with a minimum value of $-20(\pm6)\,\mathrm{kV\,m^{-1}}$ at the LCFS, green profile in fig. 3(d) at $t = 17.925\,\mathrm{s}$, with the v_ϕ component providing 65% of the value of the minimum in E_r.

On entering the ELM-free phase the plasma edge $\bar{n}_e$ continues to increase at a rate similar to that during the initial ELMy phase and the value of H_{98} increases from 1.0 to a maximum of 1.1 at 18.4 s, as seen in fig. 1. Both the T_e and T_i pedestals continue to develop during the ELM-free H-mode, with the top of pedestals reaching maximum values of $T_i = 1500(\pm15)\,\mathrm{eV}$ and $T_e = 870(\pm87)\,\mathrm{eV}$ both at $\rho = 0.94$ (blue profiles), shown in figs. 5 and 6. The v_θ profile demonstrates a great deal of evolution during the ELM-free phase, with the development of a sheared region of rotation across the T_i pedestal, as shown in fig. 5(d). Just within the LCFS, v_θ decreases to around $2\,\mathrm{km\,s^{-1}}$ as the T_i gradient region moves further in towards the core plasma, as shown by the green and red profiles in fig. 5(d) and by the black time-trace in fig. 6(d). Over the same time period the channels closest to the pedestal top measure a gradual increase in v_θ to a maximum of $7.0(\pm1)\,\mathrm{km\,s^{-1}}$ in the electron diamagnetic direction, see fig. 5(d) and red trace in fig. 6(d). At the same time, the innermost channel shown, see green and blue time traces in fig. 6(d), increases to a maximum of $-6(\pm2)\,\mathrm{km\,s^{-1}}$ in the ion diamagnetic direction. As shown by the red profile in fig. 5(d) the overall effect is the development of a well-like structure in the v_θ profile across the edge plasma. The v_ϕ profile continues to develop during the ELM-free phase with spin-up in the co-current direction. While the region close to LCFS demonstrates relatively little increase in v_ϕ, the inner channels measure an increase from $-9.6(\pm7)\,\mathrm{km\,s^{-1}}$ to $-88(\pm4)\,\mathrm{km\,s^{-1}}$ at 9 cm from the LCFS, as seen in the red and blue profiles of fig. 5. The outermost channels on the other hand measure a small increase of $29(\pm3)\,\mathrm{km\,s^{-1}}$ over this time, resulting in steepening of the edge v_ϕ gradient. The profiles of E_r over this phase become more positive as v_θ profile increases across the edge plasma. The result is a steeper E_r gradient in the edge region, with the pressure and v_θ terms provide similar contributions in the pedestal region.

The first of three very large ELMs occurs at $t = 18.9\,\mathrm{s}$. The T_i, T_e, v_ϕ, v_θ and E_r profiles across the second ELM are plotted in fig. 7 and the corresponding time-traces over all three ELMs are shown in fig. 8, for the corresponding radial locations. The three large ELMs were characterised by decreases in plasma energy 1.1 MJ, 1.4 MJ and 1.2 MJ, respectively. Comparing the T_i profiles prior to the second large ELM (black and red profiles) with that directly after (blue profile), a decrease in T_i is first observed within 4 cm of the LCFS, while the inner region maintains pre-ELM values. In the subsequent time-slice 50 ms later, the inner channels also measure a decrease in T_i (green profile) and the overall decrease in T_i is from $1373(\pm28)\,\mathrm{eV}$ at 20.075 s to $908(\pm13.2)\,\mathrm{eV}$ at 20.175 s at the pedestal top. As shown in fig. 7(b) the pedestal T_e also falls from $860(\pm86)\,\mathrm{eV}$ to a minimum of $200(\pm20)\,\mathrm{eV}$ following the ELM. These

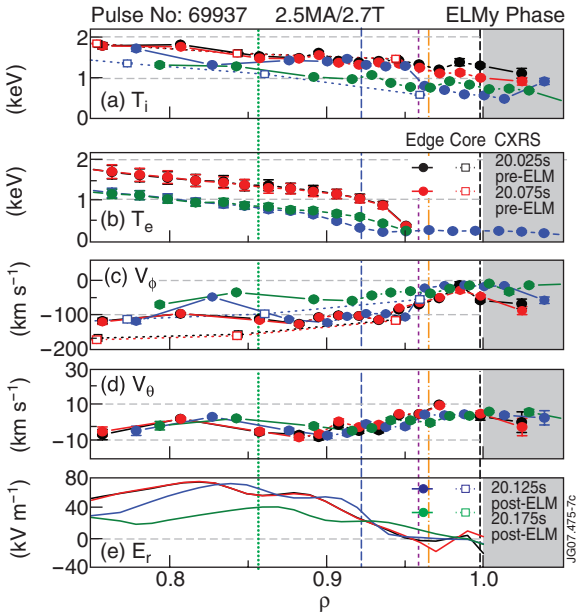

Fig. 7: Radial profiles of (a) T_i, (b) T_e, (c) v_ϕ, (d) v_θ and (e) E_r before and following a large ELM indicated in fig. 8, for shot # 69937.

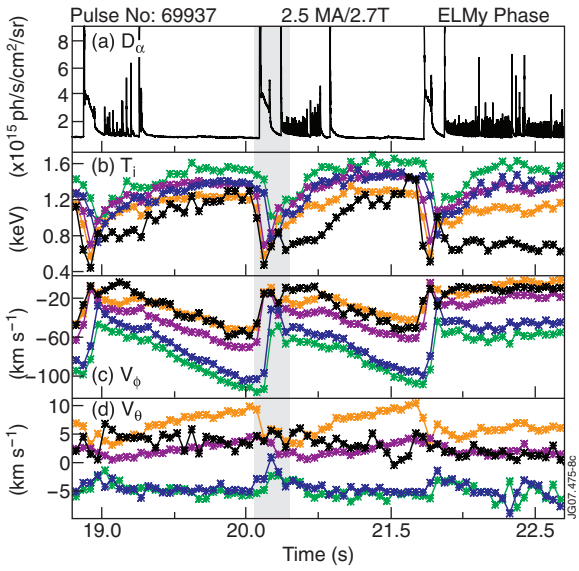

Fig. 8: Time traces across the large ELMs phase of the H-mode for shot # 69937.

large ELMs also have a significant effect on the v_ϕ rotation profile, shown in fig. 7(c), with the region 4 cm inside the LCFS the first to demonstrate a decrease in v_ϕ by a maximum of 56 km s^{-1}, (blue profile). In the following time-slice (green profile) the remainder of the edge v_ϕ profile is also reduced with the mitigation of the edge v_ϕ gradient. The v_θ time traces also demonstrate a slowing down following the ELMs, with the most sensitive channels within the T_i gradient region and can be seen in figs. 2(d) and 8(d) to drop by 5($\pm$0.5) km s^{-1} in v_θ over each large ELM. Despite these changes the overall v_θ profile is largely

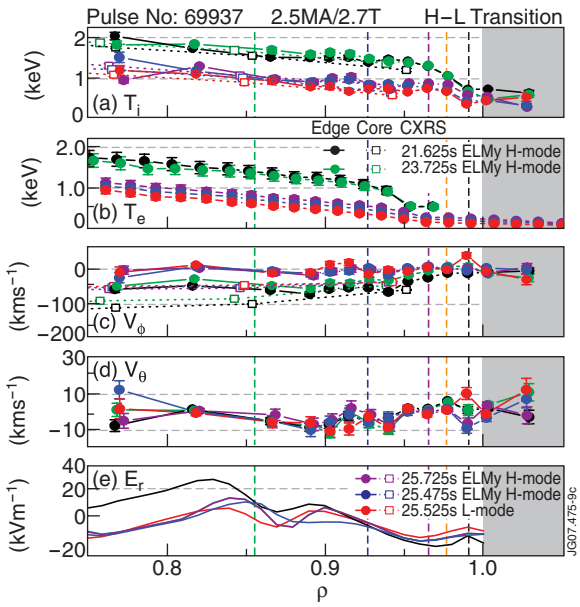

Fig. 9: Radial profiles at the start of the high frequency ELM phase and across the H-L transition for shot # 69937, for times indicated by vertical colour lines in fig. 10.

unaffected by the ELMs. The corresponding profiles of E_r shown in fig. 7(e), show a degradation of the pedestal E_r gradient following the ELM, compare the red with green profiles. The main source of the reduction in E_r is from the 40% decrease of the v_ϕ term in the pedestal region following the ELM.

The input power ramp down starts at 20.4 s and the third large ELM is directly followed by a phase of high-frequency small ELMs, as shown in figs. 1, 2 and 10. The H-mode remains in this high-frequency ELMy phase until the transition to L-mode at 25.5 s. The power threshold for the H-L transition in this shot was $P_{HL} = 5.4$ MW at an edge $\bar{n}_e = 1.7 \times 10^{19}$ m^{-3}. The confinement factor at the start of the high-frequency ELMs falls to a minimum of $H_{98} = 0.9$ at 21.4 s and subsequently recovers to a maximum value of $H_{98} = 1.1$ at 22.71 s, as shown in fig. 1. The confinement factor remains at this value until 23.62 s after which it gradually falls reaching a value of $H_{98} = 1$ at the H-L transition. Comparing figs. 7 (red profile) with fig. 9 (black and green profiles) the effect of the decrease in power and the onset of high-frequency ELMs is first seen in the outermost, edge plasma, closest to the LCFS as a clear reduction in T_i. As the input power decreases further, the ELM frequency increases further, the rest of the T_i pedestal is also modified, with the pedestal T_i falling from 1310($\pm$20) eV at $\rho = 0.95$ to 700($\pm$17) eV (blue profile) at $\rho = 0.95$, the T_i barrier width shrinks from 3 cm to 2 cm. A similar change in T_e pedestal is observed with a drop in the pedestal T_e from 906($\pm$91) eV to 423($\pm$42) eV. The v_θ profiles demonstrate a general erosion of the well-like structure in the profile as the power ramps down, with a reduction of difference in v_θ to a minimum value of 8($\pm$3) km s^{-1} at 25.48 s preceding the H-L transition. The

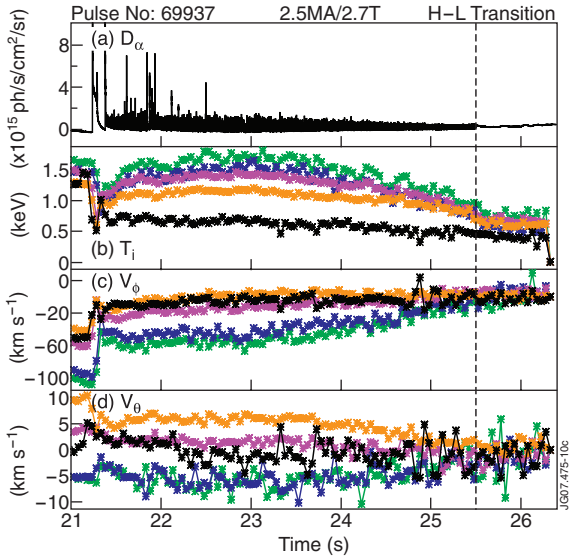

Fig. 10: Time traces across the high frequency ELM phase and the H-L transition of shot # 69937 for (a) the divertor D_α, (b) T_i, (c) v_ϕ and (d) v_θ, for radial channels indicated in fig. 9 by vertical lines in corresponding colours.

loss of shear in v_θ 300 ms before the H-L transition can also be clearly seen in the time-traces shown in fig. 10. Finally, the edge v_ϕ evolves to a very flat profile at around 0 km s^{-1} by the end of the ELMy H-mode also shown in figs. 9 and 10. The degradation of all three terms over the power ramp down contribute approximately equally to the reduction and flattening off of the E_r profile towards the end of the ELMy phase as shown by the profiles in fig. 9(e).

Conclusions. – Highly spatially resolved measurements of the edge plasma, carbon ion T_i, T_e, v_θ, v_ϕ and E_r have been documented for the first time through many different stages of a JET L- and H-mode plasma. No evidence of spin-up of v_θ prior to the L-H transition has been observed with a time resolution of 50 ms, although a clear increase in v_θ is recorded directly following the transition to H-mode. This localised spin-up precedes the onset of an ELM-free phase in which further development of the T_i, T_e, v_ϕ and v_θ profile structure is clearly seen. The E_r profile remains very flat throughout the L-mode phase and strong edge gradients only start to form during the ELM-free H-mode. The very large ELMs that follow the ELM-free phase have a significant impact on the T_i and v_ϕ profiles, eroding the pedestal gradients. Pedestal region v_θ slows down by up to 5 km s^{-1} following the large ELMs. Finally, the E_r profile has also been examined on JET over the H-L transition. The pedestal T_i, T_e, v_ϕ and v_θ all demonstrate a gradual relaxation of their gradients as the input power is ramped down and the disappearance of the edge transport barrier is preceded by the erosion any significant v_θ shear. These data suggest that the development of significant shear in E_r arises as a consequence of the high confinement phase of the plasma and is not required to enter or maintain the H-mode on JET. This important result indicates that $\mathbf{E}\times\mathbf{B}$ shear suppression of turbulence does not trigger the transport barrier formation, although it may well play a role in transport barrier sustainment and dynamics.

* * *

This work was carried out within the framework of EFDA and was partly funded by the UK EPSRC and EC under the contract of Association between EURATOM/UKAEA. The views and opinions expressed herein do not necessarily reflect those of the European Commission.

REFERENCES

[1] Ikeda K. *et al.*, *Nucl. Fusion*, **47** (2007) S18.
[2] Gohil P., Burrell K. H. and Carlstrom T. N., *Nucl. Fusion*, **38** (1998) 93.
[3] Testa D., Garzotti L. and Giroud C., *Nucl. Fusion*, **46** (2006) 562.
[4] Solomon W. M., Burrell K. H., Andre R., Baylor L. R., Budney R., Gohil P., Groebner R. J., Holcomb C. T., Houllberg W. A. and Wade M. R., *Phys. Plasmas*, **13** (2006) 056116.
[5] Kim J. *et al.*, *Phys. Rev. Lett.*, **72** (1994) 2199.
[6] Hawkes N. C. *et al.*, *Plasma Phys. Control. Fusion*, **38** (1996) 1261.
[7] Andrew Y., Hawkes N. C. and Crombe K., *Rev. Sci. Instrum.*, **77** (2006) 10E913.
[8] Hawkes N. C. and Peacock N., *Rev. Sci. Instrum.*, **63** (1992) 5164.
[9] Hawkes N. C., *Rev. Sci. Instrum.*, **68** (1997) 2051.
[10] Breger P., Flewin C., Zastrow K.-D., Davies S. J., Hawkes N. C., Konig R. W. T., Pietrzyk Z. A., Porte L., Summers D. D. R. and Von Hellerman M. G., *Plasma Phys. Control. Fusion*, **40** (1998) 347.
[11] Righi E. *et al.*, *Nucl. Fusion*, **39** (1999) 309.
[12] Andrew Y., Hawkes N. C., O'Mullane M. G., Sartori R., Beurskens M. N. A., Coffey I., Joffrin E., Loarte A., McDonald D. C., Prentice R., Saibene G., Suttrop W. and Zastrow K.-D., *Plasma Phys. Control. Fusion*, **46** (2004) 337.
[13] Andrew Y., Sartori R., Righi E., de la Luna E., Hacquin S., Howell D., Hawkes N. C., Horton L. D., Huber A., Korotkov A. and O'Mullane M. G., *Plasma Phys. Control. Fusion*, **48** (2006) 479.
[14] ITER Physics Expert Groups on CDBM, *Nucl. Fusion*, **39** (1999) 2175.